Korean J. Chem. Eng., **31**(2), 268-275 (2014)
DOI: 10.1007/s11814-013-0228-z

pISSN: 0256-1115
eISSN: 1975-7220

Preparation and electrochemical behaviour of biomass based porous carbons as electrodes for supercapacitors - a comparative investigation

Adinaveen Thambidurai*, John Kennedy Lourdusamy,†, Judith Vijaya John*, and Sekaran Ganesan*****

*Catalysis and Nanomaterials Research Laboratory, Department of Chemistry, Loyola College, Chennai 600 034, India
**Materials Division, School of Advanced Sciences, Vellore Institute of Technology (VIT) University, Chennai Campus, Chennai 600 127, India
***Central Leather Research Institute, Adayar, Chennai 600 020, India
(*Received 24 July 2013 • accepted 27 October 2013*)

Abstract−We compared the relationship of the behavior and performance of sugarcane baggase and rice straw as supercapacitor electrodes. X-ray diffraction revealed the evolution of crystallites of carbon and silica during activation at higher temperature. The morphology of the carbon samples was determined by SEM. The surface area, pore volume, and pore size distribution of carbon composites were measured. The electrochemical responses were studied by using cyclic voltammetry experiment at 25 °C in a three-electrode configuration. The specific capacitance of the sugarcane bagasse carbon electrodes was in the range 92-340 F/g, whereas for rice straw, it was found to be 56-112 F/g at scan rates of 2-3 mV/s. The sugarcane bagasse carbon exhibited better performance than rice straw carbon using H_2SO_4 as the electrolyte. However, the results clearly show that lignocellulosic wastes possess a new biomass source of carbonaceous materials for high-performance supercapacitors.

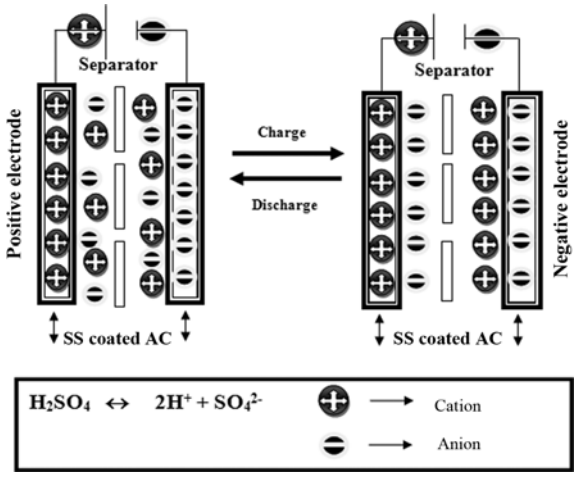

Keywords: Porous Carbon, Surface Morphology, X-ray Diffraction, Supercapacitors

INTRODUCTION

The current energy crisis necessitates a search for novel renewable and clean energy power sources. One of the regnant alternative sources of electric power is the supercapacitor. The new high current supercapacitor technology has been developed to supply or to absorb high transient energy. Usually, this kind of supercapacitor is also known as electrochemical capacitor, which electrochemically stores energy with unique properties, such as high power, long cycle life, and fast charge/discharge rates [1,2]. Generally, conducting polymers, metal oxides, and porous materials such as porous carbon, carbon aerogels and carbon nanotubes have been used as an electrode material for supercapacitors. Porous carbon (PC) is advantageous among all other possible electrode materials, because of its high surface area and porosity, good thermal and electrical conductivity, good anti-causticity, high stability, low cost and commercial-scale availability [3,4].

Porous carbon (PC) electrodes can be produced from various biomass precursors (wood, fruit shells, stones and bunches) and some fossil-fuel based precursors (petroleum and coal). Agricultural wastes are considered to be an important feedstock for preparing porous carbon (PC), among all other materials. India is the second largest producer of sugarcane after Brazil. As per the available statistics, the current sugarcane production and productivity in India are 350 million tones and 66.9 tons per hectare, respectively, and the entire crop in India is used for sugar production. Each ton of milled sugarcane gives 180-280 kg of bagasse residues [5].

Rice is the second world's largest cereal crop after wheat which

†To whom correspondence should be addressed.
E-mail: jklsac14@yahoo.co.in, jjvijayaloyola@yahoo.co.in

produces large amount of straw residues of about 330 million metric tones [6]. Thus, we made an attempt to prepare porous carbon (PC) from two different agricultural residues for comparative investigation of their properties. Among the various activation agents such as $ZnCl_2$, H_3PO_4, KOH and K_2CO_3 or their mixtures [7-9], phosphoric acid is a well known reagent for the preparation of porous carbons, which has many advantages such as non-contaminating nature [10], and highly polar character in order to control the physical and chemical interactions occurring in the bulk of the solution.

To the best of our knowledge, only few reports [11-13] exist on the preparation of porous carbon from sugarcane bagasse and rice straw based carbon for the preparation of EDLCs. Our objective is to investigate the relationship between the behavior and the performance of sugarcane baggase and rice straw based carbon as supercapacitor electrodes. From the results, it is found that the sugarcane baggase carbon is an efficient electrode material for supercapacitors than the rice straw carbon. In the present study, we investigated the structural, morphological and electrochemical properties of porous carbon. The as-prepared porous carbon was labeled as SC (sugarcane bagasse) and RS (rice straw) for comparative investigation.

EXPERIMENTAL

1. Materials

Porous carbons were prepared in the laboratory using sugarcane baggase and rice straw as the precursor material by a two-stage process: precarbonization and chemical activation. In the precarbonization process, the sugarcane baggase and rice straw were heated at 400 °C at the rate of 5 °C min^{-1} for about 4 h and cooled to room temperature at the same rate. This is labeled as precarbonized carbon (PCC). The precarbonized carbon is subjected to the chemical activation for the purpose of creating porous structure in the carbon matrix. In the chemical activation process, 50 g of the precarbonized carbon was agitated with 250 g of aqueous solution containing 85% H_3PO_4 by weight. The ratio of chemical activating agent/precarbonized carbon was fixed at 4.2. The chemical activant and precarbonized carbon was homogeneously mixed at 85 °C for 4 h. After mixing, the precarbonized carbon slurry was dried under vacuum at 110 °C for 24 h. The resulting samples were then activated heating at three different temperatures 600, 700 and 800 °C, at a heating rate of 5 °C min^{-1} using a programmer and maintained at that particular temperature for 1 h, before cooling. After cooling, the porous carbon was washed successively with hot water several times, until the pH became neutral, and successively with cold water to remove the excess phosphorous compounds. The washed samples were dried at 110 °C to get the final product. The samples activated at 600, 700 and 800 °C were labeled as SC 600, SC 700, SC 800, RS 600, RS 700 and RS 800, respectively.

2. X-ray Diffraction Studies

X-ray diffraction studies were performed using a Phillips X-pert diffractometer for 2θ values ranging from 10 to 80° using CuKα radiation at a wavelength of λ=1.540 °A. The other experimental conditions included ½° divergence slits, a 5-s residence time at each step and intensity measurements in counts.

3. N_2 Adsorption - Desorption

N_2 adsorption - desorption isotherms of the porous carbons were measured using an automatic adsorption instrument (Quantachrome Corp., Nova-1000 gas sorption analyzer) for the determination of the surface area and the total pore volumes. Prior to measurement, the carbon samples were degassed at 150 °C overnight. The nitrogen adsorption-desorption data were recorded at liquid nitrogen temperature, 77 K. The surface areas were calculated using the BET equation, which is the most widely used model for determining the specific surface area. In addition, the t-plot method [14] was applied to calculate the micropore volume and external surface area (mesoporous surface area). The total pore volume was estimated to be the liquid volume of adsorbate at a relative pressure of 0.99. All surface area measurements were calculated from the nitrogen adsorption isotherms by assuming the area of the nitrogen molecule to be 0.162 nm [15].

4. Surface Morphology

Surface morphologies of the samples were observed using Leo-JEOL scanning electron microscope. The carbon composite samples were coated with gold by a gold sputtering device for clear visibility of the surface morphology.

5. Electrochemical Measurements

Electrodes were prepared by mixing 95 wt% porous carbon and 5 wt% polyvinylidenefluoride in ethanol to form a paste, and then the slurry was then coated onto stainless steel plate, which served as a current collector. The coated electrode was dried at 70 °C in an oven for 2 h to remove the organic solvents, and then the electrode weight was measured to determine the amount of carbon coated on the stainless steel plate. The typical mass of electrode material was 0.5 mg. The electrochemical characterization of SC and RS was performed using Autolab model PGSTAT 302 N, with a three electrode system. The carbon coated on the stainless steel plate, Ag/AgCl and platinum wire was used as the working, reference and counter electrode, respectively. Cyclic voltammetry (CV) of these electrodes was performed in 1 M H_2SO_4 electrolyte.

RESULTS AND DISCUSSION

1. X-ray Diffraction Studies

The X-ray diffraction technique provides valuable information about the distribution of the active metal in the pore structure of the carbon support used in this study. The internal structure of the carbon is considered to be the most important factor [16]. Fig. 1(a), (b) shows the X-ray diffraction pattern of SC and RS carbon prepared before and after H_3PO_4 treatment. Both SC and RS consist of cellulose, lignin, hemicelluloses, ash content and volatile matters, but RS contains an ash content of 18.2% (mainly silica), in an average, which is relatively higher in comparison to other agricultural waste materials. RS is low in lignin and high in Si and K [17-19], which gives rise to a high content of SiO_2. The peaks corresponding to 2θ=23.18° indicate that the carbon can be regarded as a partly graphitized carbon, as shown in the Fig. 1(a), (b). The peak observed at 24° corresponds to tridymite [20]. In addition, a sharp peak was observed at 2θ=26° and a very small one at 2θ=43° indicating the formation of (002) and (100/101) planes corresponding to the graphitic structure. This indicates the development of atomic order and crystallite size in the increasingly carbonized carbon, which was accelerated by the increasing charring temperature. As the temperature increases from 600-800 °C, the peak becomes sharper and stronger, thus indicating a better crystallization and increase in the crystallize

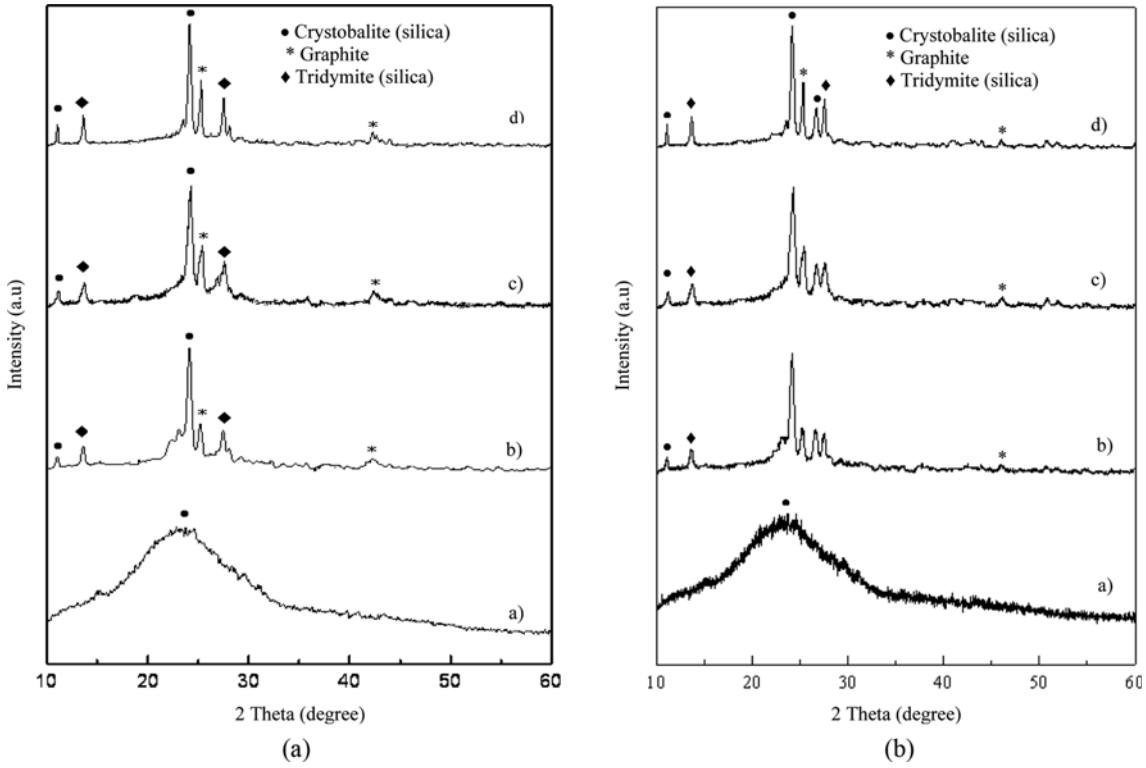

Fig. 1. (a) X-ray diffraction curves of (a) precarbonized carbon, (b) SC 600, (c) SC 700 and (d) SC 800 carbons. (b) X-ray diffraction curves of (a) precarbonized carbon, (b) RS 600, (c) RS 700 and (d) RS 800 carbons.

size. The acid-treatment and activation temperature employed were responsible for the growth of crystalline structures.

The above results suggest that the process for the preparation of porous carbons adopted could produce carbons with sp^2 and sp^3 characters in addition to the silica counter parts. Hence, compared to RS, SC reveals high graphitic planes with less silica content. As SiO_2 is well known as an insulator, the conduction property of RS carbon is very low when compared with SC carbon. All the above findings confirmed the formation of more stable graphitic carbon at higher temperature with longer residence times. The temperature employed for the activation of the precursor material can be cited as the reason for the formation of the small graphitic structures and for the crystallization of silica.

2. Nitrogen Adsorption-desorption Isotherms

The specific surface area and porosity of the carbon samples were determined by N_2 adsorption-desorption isotherms, as shown in Fig. 2(a), (b). These isotherms exhibit characteristics of typical Type-I isotherm according to IUPAC classification, with a well-defined plateau pointing to microporous structures, as the adsorption and desorption remain nearly horizontal and parallel over a wide range of relative pressures, which is the characteristic behavior of microporous materials. The appearance of a round knee at relative pressure ($0.05<P/P_o<0.15$) shows the formation of monolayer and also the gradual filling of the wider micropores. The rapid vertical rise near $P/P_0=1$ can be identified as 'cold spots' in the apparatus (which lead to bulk condensation of the gas and a false measure of adsorption in the volumetric method) [21]. The surface area parameters like BET surface area, micro and mesopore surface area, total pore volume, micro and mesopore volume and average pore diameter for both SC and RS are given in Table 1.

According to the definition by IUPAC, the adsorbent pores were classified into three groups: micropore (diameter <2 nm), mesopore (2-50 nm), and macropore (>50 nm). In general, micropores account for over 95% of the total surface area of common activated carbons [22]. The specific surface area was calculated using BET model (Table 1). The BET surface area of the precarbonized carbon of SC and RS had a low value of 169.60 m^2/g and 135.06 m^2/g, respectively. This value indicates that without the addition of suitable activation agents, it is not possible to release the bound volatile components present in the carbon matrix. The purpose of precarbonization was only to convert the lignocellulose components in the precursor into a rigid carbon structure. However, the results of the surface area parameters increased after the addition of activation agents employed at different activation temperatures.

The BET surface area of the SC 600 and RS 600 was increased to 676.95 m^2/g and 396.03 m^2/g with increase in the activation temperature. This may be attributed to the creation of slit or cylindrical pores covering both the microporous and mesoporous ranges, and shall be attributed to the pores generated on both carbon and silica components. The decrease in the surface area for SC 700 (592.46 m^2/g), RS 700 (343.89 m^2/g) and SC 800 (459.41 m^2/g), RS 800 (339.62 m^2/g) compared to SC 600 and RS 600 could be due to the pore contraction or the activation agents probably deposited in the inner pores and voids of the carbon matrix.

Activation of the sugarcane bagasse (SC) and rice straw (RS) carbon by phosphoric acid was generally more effective for introducing the mesopores in the pore-width range of 3-8 nm. Phosphoric acid can enter into the interior of the SC carbon structure and

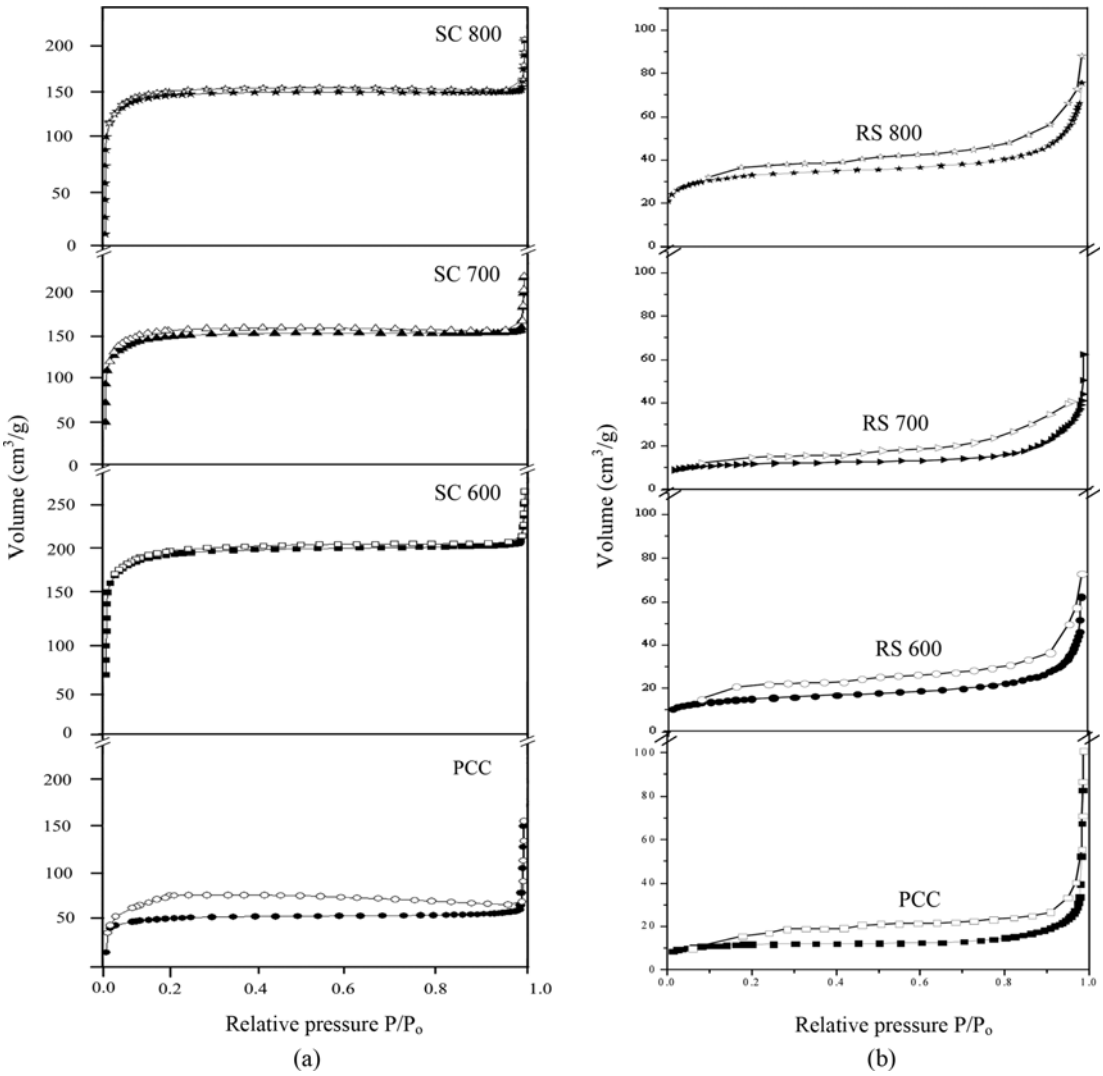

Fig. 2. (a) Adsorption-desorption isotherms of activated carbons PCC, SC 600, SC 700 and SC 800. (b) Adsorption-desorption isotherms of activated carbons PCC, RS 600, RS 700 and RS 800.

Table 1. Sample code, surface area, pore volume, average pore diameter, and production yield of sugarcane cane and rice straw derived carbon

Sample	S_{BET}[a] (m^2/g)	S_{mic}[b] (m^2/g)	S_{meso}[c] (m^2/g)	V_{Total}[d] (cm^3/g)	V_{Micro}[e] (cm^3/g)	V_{Meso}[f] (cm^3/g)	V_{Micro}/V_{Total} %	V_{Meso}/V_{Total} %	D_p[g] nm	Production yield of carbon (%)
PCC (SC)	169.60	129.84	39.75	0.246	0.052	0.194	21.1	78.8	2.9	53.00
PCC (RS)	135.06	96.04	37.13	0.196	0.042	0.154	21.4	78.5	2.7	70.79
SC 600	676.95	620.21	56.73	0.424	0.254	0.170	69.9	40.2	1.2	45.66
RS 600	376.65	330.19	46.03	0.324	0.196	0.120	60.4	37.2	1.0	65.09
SC 700	666.87	592.46	74.40	0.387	0.232	0.154	60.1	39.8	1.4	39.79
RS 700	366.57	312.46	54.40	0.287	0.175	0.112	52.4	30.7	1.2	55.89
SC 800	549.78	459.41	90.36	0.338	0.192	0.146	56.8	33.2	1.0	35.39
RS 800	349.98	279.41	70.36	0.238	0.152	0.086	43.8	26.1	0.9	45.46

[a]BET surface area
[b]Micropore surface area
[c]Mesopore surface area
[d]Total pore volume
[e]Micropore volume
[f]Mesopore volume
[g]Average pore diameter

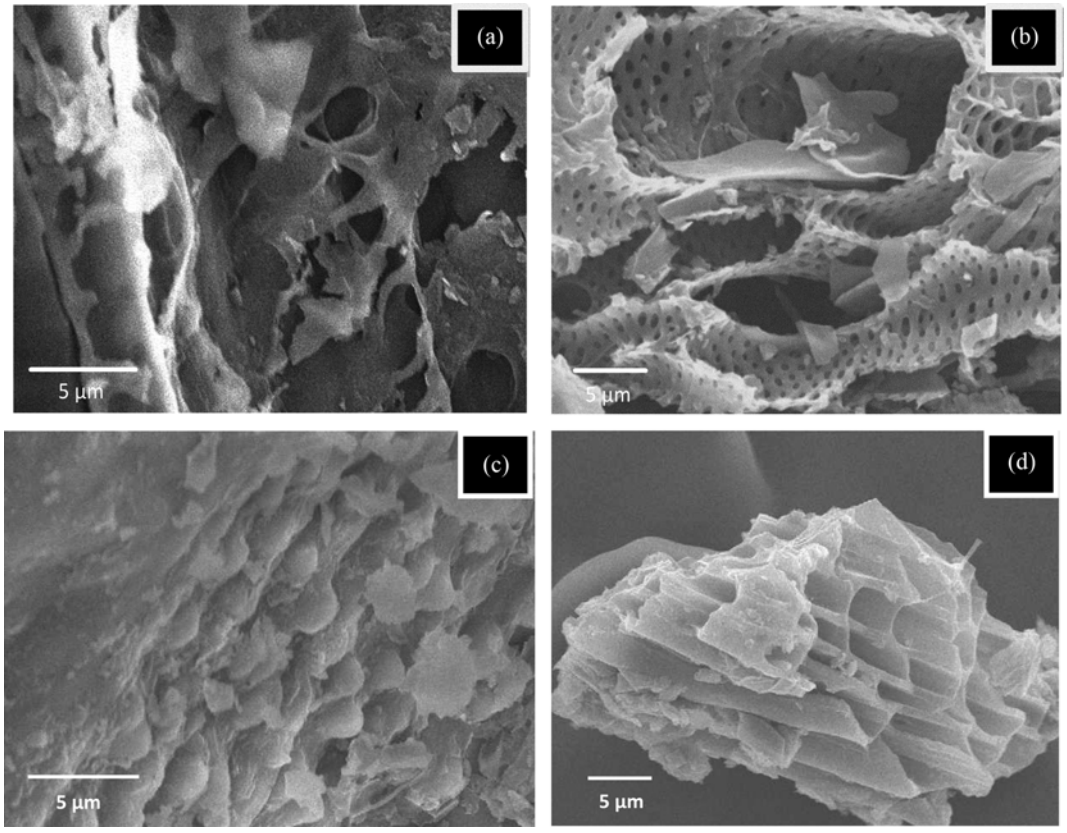

Fig. 3. (a), (b) Scanning electron micrographs of (a) precarbonized carbon (PCC) and (b) porous carbon (SC 600). (c), (d) Scanning electron micrographs of (a) precarbonized carbon (PCC) and (d) porous carbon (RS 600).

freely facilitate the activation [23]. As a result, SC activated carbon exhibited the larger mesopores carbon with a larger average pore diameter than RS activated carbon as shown in Table 1. Furthermore, increasing the activation temperature decreases the BET surface area, as observed in Fig. 2(a), (b). The mechanism is the blocking of pores by the ashes. At low activation temperature, the ashes are in the form of fine, well dispersed particles that tend together at higher activation temperatures. With such a mechanism, more porosity is blocked at high activation temperature, thereby explaining why the surface area of the carbon decreases faster with increasing temperature as reported by Fierro et al. [24].

Fig. 2(a), (b) clearly shows an increase of relative pressure (0.8) in the adsorption branch of SC carbon and a hysteresis loop at P/P_0=0.80-0.99 with a pronounced desorption step, demonstrating the mesoporous adsorption of the carbon sphere, indicating that the mesopore increases as the temperature increases. The reason is that the action of phosphoric acid on SC carbon thus essentially leads to the mesoporous activated carbons, because, micro-pores would be burnt off as a result of the high preparation temperature. This is because the small pores inside the carbon walls were gradually destroyed with increasing the temperature as observed by Chunzhong Li et al. [25].

After the activation process, the mesopore size distributions of the RS and SC increased gradually; on the other hand, their mesopore volumes decreased significantly. The decrease in the mesopore volumes occurred because mesopores can provide more reaction sites with phosphoric acid, which results in the severe collapse of mesopore volume [26]. The phosphoric acid activation induces the chemical and structural alterations of the different constituent biopolymers of the precursors, namely, cellulose, hemicellulose, and lignin, leading to the development of extensive porous structures. The above observation indicates that the activating agents at lower temperatures contribute to pore drilling and pore widening effects, while at higher temperatures, the pore contraction dominates the pore drilling forces [27].

3. SEM Studies

Fig. 3(a)-(d) shows the SEM images of the SC and RS carbons before and after phosphoric acid activation. The surface morphology of PCC in Fig. 3(a), (c) shows no generation of pores and confirms that only the lignocellulose portions present in SC and RS were converted to carbon structures. The image also reveals that only the carbonization has taken place. The sample activated at 600 ºC showed better results, when compared with those activated at the other activation temperatures. The surface morphology was studied only for SC600 and RS600 sample alone, because of its high surface area.

The SEM images of SC 600 and RS 600 are shown in Fig. 3(b), (d). The activation agents and activation temperature employed have created pores on its surface. The pore diameter shown was found to be in the mesopore range (2-50 nm). Compared with PCC, SC 600 and RS 600 has many folds and deep pits, illustrating that the structure damage increases greatly, because most of the organic volatiles evolved, leaving behind the ruptured surface of activated carbon with a large number of pores. It has been made very clear that the opening of the pores in the surface at 600 ºC should be due to

the extraction of some materials, e.g., dissolution of lignins and other mineral components from the bagasse and straw during the impregnation process, so as to create, upon activation, micro and mesopores in the carbon and silica components. As a result of the creation of pores, there is an increase in both the surface area and the pore volume, which are stably created in the carbon composite [28].

4. Electrochemical Characterization

Cyclic voltammetry (CV) technique was performed in a potential range to study the electrochemical characteristics and hence to evaluate the specific capacitance of the as prepared electrode materials. Porous carbon can be used as the electrode materials in supercapacitor technology, because of their highly available charge storage sites on its porous surface. Therefore, the porous carbon samples were used as the electrode material to understand the possible application of SC and RS based carbon electrodes in energy storage and conversion devices. Fig. 4(a), (b) exhibits the typical cyclic voltammograms (CV) for SC and RS using H_2SO_4 as an electrolyte at different scan rates (2 to 3 mV/s). The effect of scan rates was investigated in order to elucidate the charge storage mechanism of the porous carbon. Clearly, the CV curves obtained at different carbon-

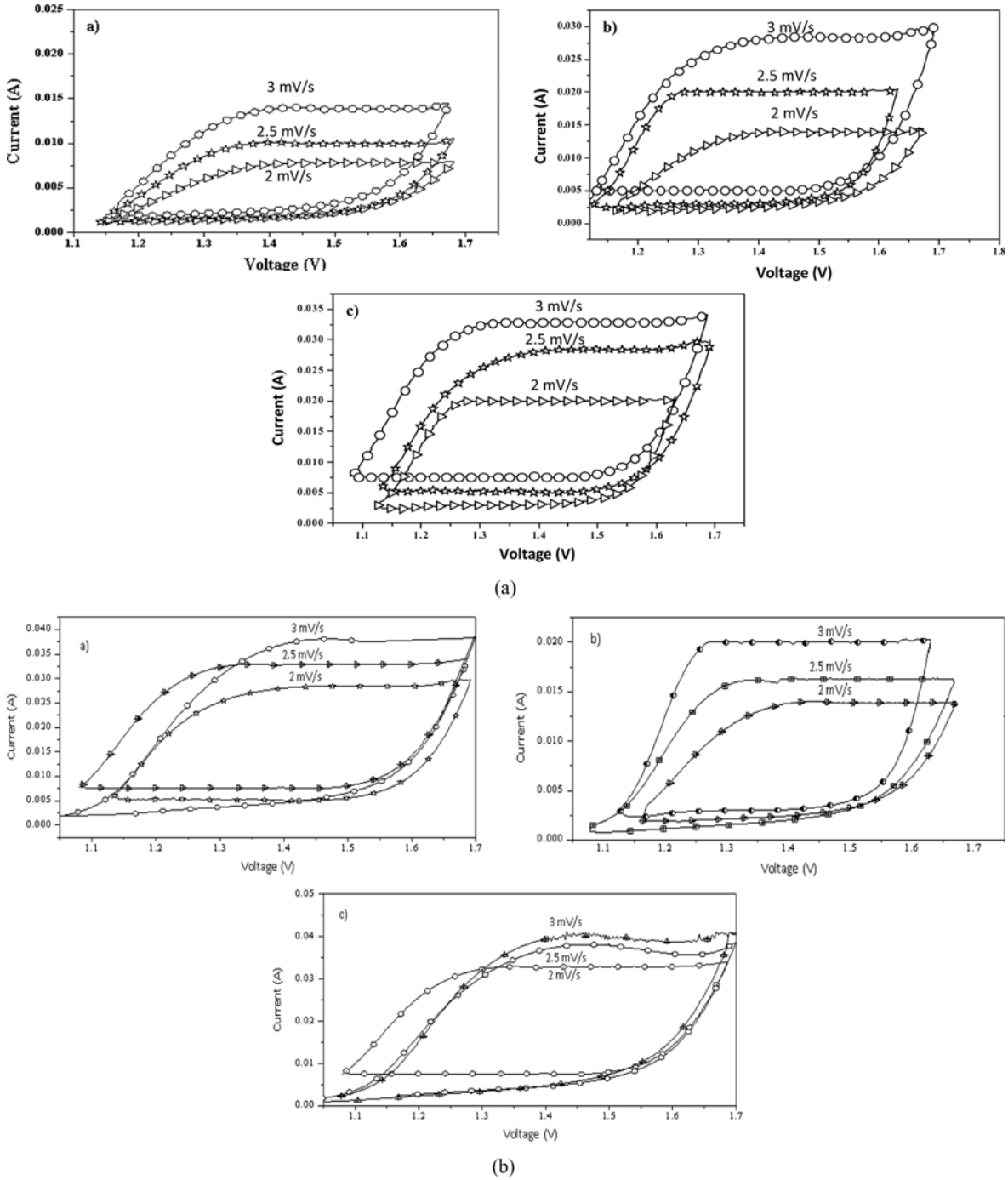

Fig. 4. (a) The cyclic voltammogram of a) SC 600 b) SC 700 and c) SC 800 using 1 M H_2SO_4 as electrolyte at different scan rates. (b) The cyclic voltammogram of a) RS 600 b) RS 700 and c) RS 800 using 1 M H_2SO_4 as electrolyte at different scan rates.

ization temperature are close to an ideal rectangular shape, evincing their better capacitive nature. This evidenced that no obvious faradic reactions occur during the charge-discharge of the electrochemical capacitor.

The specific capacitance of carbon electrode can be calculated from the cyclic voltammograms according to the following formula

$$C = \left(\frac{I_a - I_c}{2v \cdot m}\right) = \left(\frac{\Delta I}{2v \cdot m}\right) \quad (1)$$

where C is specific capacitance (F/g), v, potential scan rate (V/s), m, mass of the carbon powder, I_a and I_c, the average anodic and cathodic currents, respectively. To determine the capacitance as a function of potential, ΔI values were obtained at various potentials.

The specific capacitance of the SC carbon electrodes was in the range 92-340 F/g, whereas, for RS it was found to be 56-112 F/g at scan rates of 2-3 mV/s. Generally, the specific capacitance of the carbon electrode will increase with increase in surface area of the carbon and hence, higher surface area sugarcane bagasse carbon (676.95 m^2/g) gives higher capacitance (340 F/g) than rice straw carbon (396.03 m^2/g , 112 F/g). The presence of macropores will also be a reason for the transportation of the electrolyte ions to the bulk materials. It is suggested that the ions can occupy some of the pores in the electrode to take part in the double-layer formation. As the scan rate increases, the square potential becomes gradually depressed. Because, the ions transport into the pores more readily in lower scan rate than in higher. Thus, the specific capacitance increases with increase in BET surface area of the carbon electrode.

Since, the specific capacitance is proportional to the integral area surrounded by CV curves, we conclude that the sequence of capacitance values was: 600 ºC>700 ºC>800 ºC for both SC and RS carbon electrodes. However, it may also depend on pores and if the pore contraction occurs, it is unfavorable for the ions to penetrate into the deeper region, which is the reason for the decrease in capacitance as the temperature increases. Therefore, its surface may not be completely utilized for charge storage as the activation temperature increases.

The stability of SC and RS during the charge-discharge cycling at current densities of approximately 5 A/g that represents a current density for a high power application is presented in Fig. 5. For RS, the capacitance drops after 2500 cycles to 73% of the first cycle, but after 5000 cycles the capacitance falls by only another 5% of the capacitance in the first cycle. SC shows better stability with 81% of the capacitance retained after 2500 cycles; however, after 5000 cycles the capacitance falls by only another 2% of the capacitance in the first cycle. The cycling performance of both RS and SC is comparable with other biomass-derived activated carbon electrodes reported in the literature [29], but in the present study the cycling performance is measured at a much higher current load. However, the prepared carbon electrode shows excellent reversibility and stability. This clearly indicates the ideal double-layer behavior and the excellent supercapacitor performance of H_3PO_4 activated SC than RS as an electrode material for energy storage devices [12].

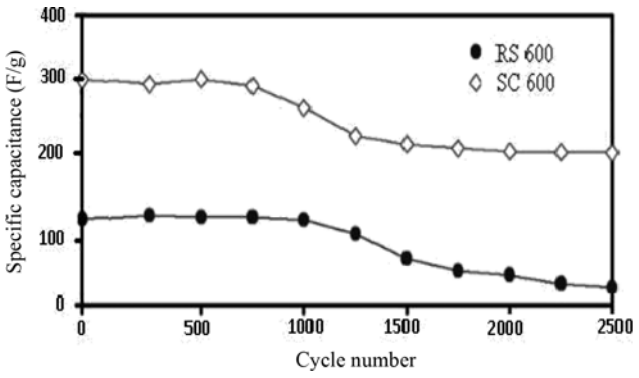

Fig. 5. Charge-discharge cycling stability of RS 600 and SC 600 at a current load of 20 mA. Specific capacitance is calculated from the discharge profiles of the galvanostatic cycling curve.

Rufford et al. [11] reported the electrochemical performance of activated carbon electrodes prepared by $ZnCl_2$ activation of sugar cane carbon, that has displayed the excellent electro-chemical properties with specific capacitances as high as 300 F/g observed in supercapacitor cells containing 1 M H_2SO_4 electrolyte. Zhuo et al. [30, 31] reported the activated carbon electrodes prepared by $ZnCl_2$ activation of sugar cane, which could deliver 9.2 Wh/kg of energy density, while maintaining 2.5 kW/kg of power density with specific capacitance of 320 F/g. However, the specific capacitance of the sugarcane bagasse carbon electrodes prepared by phosphoric acid activation in the present study is 340 F/g, which is relatively higher than the other reported works [11,30,31]. Moreover, there is no literature found for the supercapacitor electrode preparation by using the rice straw.

CONCLUSIONS

The formation of slight crystallinity in the porous carbon structure and crystalline silica was noted through XRD curves. The use of H_3PO_4 has the effect of producing considerable quantities of micropores and mesopores. The inclusion process prior to chemical activation makes the process simpler and cheaper. Usually, H_3PO_4 activation temperature will be in the range of 400-700 ºC, but we used 600-800 ºC. The main cause is that we got very low specific capacitance upto 500 ºC. Similarly, 900º (sintered at 900 ºC) gave a lower specific capacitance than that of 800 ºC. It was found that the chemical activation at 600 ºC is optimum to produce high surface area for both SC and RS. We have demonstrated an environmentally friendly approach for the fabrication of electrical double layer capacitors (EDLCs) using sugarcane bagasse and rice straw as the possible precursor material. When compared to commercial carbon, porous carbon prepared from sugarcane bagasse in the present study has higher capacitance. The reason is that macroporous value, ionic mobility, pore size distribution and the surface chemistry made a vast specific capacitance difference with commercial carbon. The result clearly indicates the excellent supercapacitor performance of SC over RS as an electrode material for energy storage devices. These properties possibly enable these lignocellulosic wastes to act as a new biomass source of carbonaceous materials for high-performance.

ACKNOWLEDGEMENT

The corresponding author duly acknowledges the financial support by SERC Division, Department of Science and Technology (DST), New Delhi, India, through the young scientist project scheme

vide reference no. SR/FTP/PS-76/2005.

REFERENCES

1. J. R. Miller and P. Simon, *Science*, **321**, 651 (2008).
2. P. Simon and Y. Gogotsi, *Nature Materials*, **7**, 845 (2008).
3. A. G. Pandolfo and A. F. Hollenkamp, *J. Power Sources*, **157**, 11 (2006).
4. V. N. Vasile Obreja, *Physica E: Low. Dimens. Syst. Nanostruct*., **40**, 2596 (2008).
5. J. A. Pessoa, I. M. de Manchilha and S. Sato, *J. Ind. Microbio. Biotechnol*., **18**, 360 (1997).
6. P. Robinson, University of California Davis, Personal Communication (2006).
7. W. T. Tsai, C. Y. Chang and S. L. Lee, *Carbon*, **35**, 1198 (1997).
8. G. Yanping and D. A. Rockstraw, *Micropor. Mesopor. Mater*., **100**, 12 (2007).
9. J. Hayashi, H. Toshihide, T. Isao, M. Katsuhiko and N. A. Fard, *Carbon*, **40**, 2381 (2002).
10. W. C. Lim, C. Srinivasakannan and N. Balasubramanian, *J. Anal. Appl. Pyrol*., **88**, 181 (2010).
11. T. E. Rufford, D. H. Jurcakova, K. Khosla, Z. Zhu and L. Gao, *J. Power Sources*, **195**, 912 (2010).
12. H. Chun-Hisen and A. D. Ruey, *Micropor. Mesopor. Mater.*, **147**, 47 (2012).
13. F. Zhang, K. X. Wang, G. D. Li and J. S. Chen, *Electrochem. Commun*., **11**, 130 (2009).
14. I. Salame and J. B. Teresa, *J. Ind. Eng. Chem. Res.*, **39**, 301 (2000).
15. S. J Gregg and K. S. W. Sing, Adsorption, Surface Area and Porosity, Academic Press, London (1982).
16. A. C. Pastor, R. Rodriguez, H. Marsh and M. A. Martinez, *Carbon*, **37**, 1275 (1999).
17. C. Liao, C. Wu, Y. Yanyongjie and H. Huang, *Biomass. Bioenerg*., **27**, 119 (2004).
18. P. J. Van Soest, *Anim. Feed. Sci. Technol*., **130**, 137 (2006).
19. K. Raveendran, G. Anuraddha, C. Kartick and K. Khilar, *Fuel*, **74**, 1812 (1995).
20. N. Yalcin and V. Sevnic, *Ceram. Int.*, **27**, 219 (2001).
21. H. Y. Chang, H. P. Yun and R. P. Chong, *Carbon*, **39**, 559 (2001).
22. K. S. W. Sing, *Pure. Appl. Chem*., **54**, 2201 (1982).
23. Y. Guo, S. Yang and Z. Wang, *Mater. Chem. Phys*., **74**, 320 (2002).
24. V. Fierro, G. Muñiz, A. H. Basta, H. El-Saied and A. Celzard, *J. Hazard. Mater*., **181**, 27 (2010).
25. Z. Zhu, Y. Hu, H. Jiang and C. Li, *J. Power Sources*, **246**, 402 (2014).
26. E. Jeong, M. J. Jung and Y. K. Lee, *J. Fluorine Chem.*, **150**, 98 (2013).
27. W. T. Tsai, C. Y. Chang, M. C. Lin, S. F. Chien, H. F. Sun and M. F. Hsieh, *Chemosphere*, **45**, 51 (2001).
28. T. Adinaveen, L. J. Kennedy, J. J. Vijaya and G. Sekeran, *J. Ind. Eng. Chem.*, **19**, 1470 (2013).
29. V. Subramanian, C. Luo, A. M. Stephan, K. S. Nahm, S. Thomas and B. Wei, *J. Phys. Chem. C*, **111**, 7527 (2007).
30. W. J. Si, X. Z. Wu, W. Xing, J. Zhou and S. P. Zhuo, *J. Inorg. Mater*., **26**, 107 (2011).
31. X. Z. Wu, J. Zhou, W. Xing and S. P. Zhuo, *J. North Uni. China*, **33**, 179 (2012).